Deterministic access of broadband frequency combs in microresonators using cnoidal waves in the soliton crystal limit

ZHEN QI,[1,*] AMIR LESHEM,[2] JOSE A. JARAMILLO-VILLEGAS,[3] GIUSEPPE D'AGUANNO,[1] THOMAS F. CARRUTHERS,[1] OMRI GAT,[2] ANDREW M. WEINER,[4] AND CURTIS R. MENYUK[1]

[1]*University of Maryland at Baltimore County, 1000 Hilltop Circle, Baltimore, MD 21250, USA*
[2]*Hebrew University of Jerusalem, Jerusalem 91904, Israel*
[3]*Universidad Tecnologica de Pereira, Cra. 27 10-02, Pereira, Risaralda 660003, Colombia*
[4]*Purdue University, 610 Purdue Mall, West Lafayette, IN 47907, USA*
[*]*zhenqi1@umbc.edu*

Abstract: We present a method to deterministically obtain broad bandwidth frequency combs in microresonators. These broadband frequency combs correspond to cnoidal waves in the limit when they can be considered soliton crystals or single solitons. The method relies on moving adiabatically through the (frequency detuning)×(pump amplitude) parameter space, while avoiding the chaotic regime. We consider in detail Si_3N_4 microresonators with small or intermediate dimensions and an SiO_2 microresonator with large dimensions, corresponding to prior experimental work. We also discuss the impact of thermal effects on the stable regions for the cnoidal waves. Their principal effect is to increase the detuning for all the stable regions, but they also skew the stable regions, since higher pump power corresponds to higher power and hence increased temperature and detuning. The change in the detuning is smaller for single solitons than it is for soliton crystals. Without temperature effects, the stable regions for single solitons and soliton crystals almost completely overlap. When thermal effects are included, the stable region for single solitons separates from the stable regions for the soliton crystals, explaining in part the effectiveness of backwards-detuning to obtaining single solitons.

1. Introduction

Broadband optical frequency combs in which all the frequency modes are coherently locked make it possible to measure frequency with great accuracy and have enabled a wide range of applications [1]. These include applications to basic science, astrophysics, environmental and chemical sensing, medicine, and military technology [2,3]. However, frequency combs are usually produced using passively modelocked lasers and are often bulky and expensive. It was discovered in 2007 that it is possible to produce broadband frequency combs in microresonators [4,5], which are μm-size or mm-size optical rings. This discovery opened up the prospect of compact, relatively inexpensive frequency combs and led to a worldwide effort to obtain an octave of bandwidth and lock the frequency combs [6]. Microresonator frequency combs are produced by a microresonator to which an optical waveguide carrying continuous wave light is coupled. The light from this waveguide pumps a single resonant frequency mode inside the microresonator. This mode then parametrically pumps other microresonator modes [7,8], ultimately creating a broadband comb [9,10]. However, this comb is typically incoherent and corresponds to a randomly fluctuating optical amplitude inside the microresonator. The most common approach to generate a coherent comb is to either tune the pump frequency [11–16] or the pump power [13,17,18]. When successful, this process generates a single (bright) soliton that circulates in the cavity—corresponding to a coherent comb. However, this process is not

deterministic. Most of the time it does not produce a single soliton, and the process must be repeated multiple times until a single soliton is randomly obtained.

This approach has achieved notable successes in recent years. These have included the demonstration that an octave of bandwidth can be obtained [19], the demonstration of an on-chip optical frequency synthesizer [20], demonstration of microwave purification [21] and microwave synthesis [22], and applications to dual-comb spectroscopy [23] and lidar [24,25]. However, this approach has significant drawbacks. As noted, the single soliton generation is random. Indeed, recent work has demonstrated that when thermal effects can be neglected there is no path through the parameter space that can deterministically generate single solitons because continuous waves and multiple soliton solutions that are soliton crystals co-exist in the parameter space [26].

Another drawback of single solitons is that they use the pump inefficiently. Less than 1% of the pump power typically goes into the frequency comb [14]. Associated with this drawback is another; single solitons are thermally unstable unless the device temperature is carefully managed. When a single soliton is generated, the device cools, and the soliton can become unstable. To avoid this instability, a feedback control system is required, which adds to the system complexity [27]. There have been several recent proposals for the deterministic generation of solitons. In one approach, multiple pump frequencies are used to modulate the input pump amplitude [28–31] or phase [32]. This approach has been demonstrated experimentally [33–35]. Another approach is to add an additional ring [36–38] or an additional mode interaction in the same ring [39]. All these approaches require significant additional hardware and seriously complicate the design of the frequency comb generator. In all of these approaches, careful management of the thermal instability is required.

Here, we describe a method for deterministic generation of a broadband frequency comb that overcomes the disadvantages of the current approaches to single soliton generation without requiring a significant increase in the hardware complexity. In general, our method creates a broadband frequency comb by generating a periodic array of solitons or a perfect soliton crystal rather than a single soliton. Soliton crystals have been the subject of increasing study in the past three years [26,40–49] and have advantages over single solitons. First, soliton crystals use the pump N times more efficiently than a single soliton, where N is the number of solitons in the crystal, and the power in the frequency comb increases by a factor N. Second, the number of frequency comb lines is reduced by a factor N, and the power in each comb line is multiplied by a factor N^2 [26]. By adiabatically following an appropriate path through the parameter space that consists of (frequency detuning)×(pump amplitude), it is possible to first generate a narrowband cnoidal wave that corresponds to periodically-spaced peaks on top of a high pedestal. As the system parameters continue along the access path, the narrowband cnoidal wave continuously transforms into a broadband cnoidal wave that is effectively a stable, periodic array of solitons, i.e., a soliton crystal [26].

In this paper, we use "soliton crystal" to denote perfect soliton crystals. These are periodic waveforms in the microresonator and hence cnoidal waves. Soliton crystals with defects [40] are not periodic waveforms, and hence are not cnoidal waves.

We previously described a deterministic approach for generating broadband cnoidal waves when thermal effects can be neglected. However, in practical systems, thermal effects are almost never negligible, although there are exceptions [50]. We will show that this approach must be modified when we take into account thermal effects, and the path through the parameter space becomes slightly more complicated. However, the basic approach remains the same. This work extends and describes in more detail previous work that appeared in [51].

This method for generating broadband frequency combs is thermally stable. Since the generation of the soliton crystal or single soliton is deterministic, we need merely move adiabatically along the deterministic path in the parameter space, i.e., move at a speed that is sufficiently slow to ensure that the system is in thermal equilibrium at each point in the parameter space.

2. Basic equations and system parameters

The equation that describes the evolution of the light envelope in the microresonator is the modified Lugiato-Lefever equation (LLE) that may be written [52]

$$
\begin{aligned}
T_R \frac{\partial \Psi}{\partial \tau} &= -i\frac{\beta_2}{2}\frac{\partial^2 \Psi}{\partial \theta^2} + i\gamma|\Psi|^2\Psi + \left\{-i\left[\omega_r(T)-\omega_0\right]T_R - \frac{l}{2}\right\}\Psi + i\sqrt{P_{\text{in}}},\\
\frac{\partial \Delta T}{\partial \tau} &= \frac{\lambda}{2\pi}\int_{-\pi}^{\pi}|\Psi(\theta)|^2 d\theta - \kappa\Delta T,
\end{aligned}
\tag{1}
$$

where $\Psi(\tau,\theta)$ is the slowly varying envelope of the optical amplitude, T_R is the round-trip time, τ is time, $\theta=[-\pi,\pi]$ is the azimuthal coordinate, β_2 is the group velocity dispersion (GVD) coefficient in (radians)^2/round-trip, γ is the nonlinear Kerr coefficient, l is the linear power loss per round trip, ω_0 is the angular frequency of pump, $\omega_r(T)$ is the angular frequency of the resonator mode at the cavity temperature T, P_{in} is the pump power that resides in the transverse microresonator mode, $\Delta T = T - T_0$ is temperature difference between the cavity temperature T and the ambient temperature T_0, λ is the thermal absorption coefficient, and κ is the thermal relaxation coefficient reported in the references given in Table 1. We note that Eq. (1) is valid for microresonators that are made using silicon nitride or other ceramic materials. Microresonators that are made using crystalline materials like CaF have a more complicated thermal behavior [53]. Thermal effects are often neglected in theoretical studies of microresonators. While they do not impact the existence of stable cnoidal waves solutions, they do significantly affect the location of the stable regions in the (frequency detuning)×(pump amplitude) parameter space. In particular, they cause the stable region for single solitons to become separate from the stable regions for soliton crystals [51].

Table 1. Parameters for three experimentally demonstrated silicon-nitride microresonators or silica microresonators with relatively small [50], intermediate [54], and large [13] mode circumferences and hence three different values of the free spectral range (FSR).

Parameter	[50]	[54]	[13]
Material	Si_3N_4	Si_3N_4	SiO_2
$R\ [\mu\text{m}]$	23	100	1500
FSR [GHz]	1004	240	22
T_R [ps]	1.00	4.16	45.4
β_2	-3.19×10^{-4}	-8.74×10^{-5}	-4.85×10^{-6}
$\gamma\ [\text{W}^{-1}]$	1.31×10^{-4}	8.80×10^{-4}	1.59×10^{-5}
l	3.22×10^{-3}	3.70×10^{-3}	5.52×10^{-4}
λ [K/J]	8.70×10^{3}	7.22×10^{5}	0.25
κ [MHz]	0.29	10	1×10^{-3}
A	-6.13×10^{-4}	-0.12	-9.38×10^{-4}
B	1.79×10^{-4}	0.022	1.65×10^{-4}
C	3.42	5.12	5.7
L	20.0	40.9	67.0
P_{in}/F^2 [mW]	15.8	3.89	4.78
f_{det}/α [MHz]	257	70.8	0.97

After normalization, Eq. (1) becomes

$$\frac{\partial \psi}{\partial t} = i\frac{\partial^2 \psi}{\partial x^2} + i|\psi|^2\psi - [1 + i(\alpha + \Phi)]\psi + F,$$
$$\frac{\partial \Phi}{\partial t} = AP - B\Phi, \tag{2}$$

where $\psi = (2\gamma/l)^{1/2}\Psi$ is the normalized slowly varying envelope of the optical amplitude, $t = [l/(2T_R)]\tau$ is the normalized time, $x = (l/|\beta_2|)^{1/2}\theta$ is the normalized azimuthal coordinate. We have $-L/2 < x < L/2$, where $L = 2\pi(l/|\beta_2|)^{1/2}$ is the longitudinal mode circumference, normalized to the dispersive scale length [26]. The quantity $\alpha = 2[\omega_r(T_0) - \omega_0]T_R/l$ is the normalized angular frequency detuning between the cavity resonance and the pump laser. The physical frequency detuning f_{det} is given by $f_{\text{det}} = [\omega_r(T_0) - \omega_0]/(2\pi) = [l/(4\pi T_R)]\alpha$. The normalized thermal detuning is given by $\Phi = 2[\omega_r(T) - \omega_r(T_0)]T_R/l = M\Delta T$, where $M = 2\omega_r(T_0)T_R(\partial n/\partial T)/(nl)$ and $n(T)$ is the refractive index. We are assuming that the temperature change is small so that a Taylor expansion of $n(T)$ is valid. The normalized pump amplitude is given by $F = i(8\gamma P_{\text{in}}/l^3)^{1/2}$, and $P = (1/L)\int_{-L/2}^{L/2}|\psi(x)|^2 dx$ is the normalized average intracavity power in the frequency comb. The normalized thermal coefficients $A = \lambda T_R M/\gamma$ and $B = 2T_R\kappa/l$ give the shift of the detuning in response to the intracavity power and the thermal relaxation rate, respectively. It is useful to define the ratio $C = -A/B$. For the stationary solutions of Eq. (2), we have $\Phi = -CP$. Hence, the stationary solution with a fixed value of $\alpha - CP$ and a fixed value of F is the same for any value of the thermal ratio C. The parameter B governs the rate at which a thermal perturbation relaxes and hence it is necessary to move through the parameter space at a rate that is small compared to B in order for the evolution to be adiabatic. In physical units for the parameters of [54], we find that the relaxation rate is $[0.1\ \mu s]^{-1}$ as shown in Table 1. So, the evolution through the parameter space must be slow compared to $0.1\ \mu s$. For the other example systems in Table 1, we find for the parameters in [50] that the evolution should be slow compared to $3.4\ \mu s$, while for the parameters in [13] the evolution should be slow compared to 1 ms.

In [26], we describe in detail the computational methods that we used to solve Eq. (2). We use boundary-tracking algorithms based on dynamical methods to find the stable regions. We use efficient split-step methods, combined with quantum noise, to find the time evolution.

In Table 1, we show parameters for three experimentally demonstrated silicon-nitride microresonators or silica microresonators with relatively small [50], medium [54], and large [13] mode circumferences and hence three different values of the free spectral range (FSR). We assume that all devices are operating at room temperature and are pumped at $1.5\ \mu m$.

3. Results

In Fig. 1, we show the stable regions when $L = 50$ for different cnoidal wave periodicities N, both with and without thermal effects. We recall that a cnoidal wave is a periodic waveform whose azimuthal period equals $2\pi/N$, where the periodicity N can be any positive integer [26]. When $N = 1$, the cnoidal wave corresponds to a single soliton. For $N \lesssim L/(2\pi)$, we found that cnoidal waves correspond approximately to a periodic string of solitons, while when $N \gtrsim L/(2\pi)$, the cnoidal waves correspond to Turing rolls in which the periodically varying amplitude sits atop a pedestal of comparable magnitude. The choice $L = 50$ in Fig. 1 corresponds approximately to the experiments of Wang et al. [14]. The periodicities of the stable regions scale linearly with L [26] so that the regions in (α, F) that are stable for periodicity N_1 with $L = L_1$ are approximately the same as the regions that are stable for periodicity $N_2 = cN_1$ when $L = L_2 = cL_1$. The observed scaling with L is physically reasonable since an increase in L corresponds to an increase in the mode circumference, so that the physical length of the cnoidal wave period remains approximately constant as both L and periodicity N increase. Figure 1(a) shows the stable regions with no

thermal effect ($C = 0$), while Fig. 1(b) shows the stable regions with $C = 5$, which corresponds to the coefficient for silicon nitride at room temperature [54]. Comparing Figs. 1(a) and 1(b), we see that thermal effects shift all the stable regions to larger detuning frequencies (larger α and lower pump frequencies). The regions are also stretched and skewed. When thermal effects are not included, the stable regions for low periodicities ($N \leq 5$ with $L = 50$) almost completely overlap. That is no longer true when thermal effects are included. Cnoidal waves with a low periodicity correspond to a periodic stream of solitons, i.e., a soliton crystal [26,40–49], so that the stable regions are expected to overlap when thermal effects are not included. However, the intracavity power is approximately proportional to the periodicity, so that when thermal effects are included the detuning of the stable regions decreases as the periodicity decreases. We observe that there is a parameter regime in which stable single solitons exist, but stable soliton crystals do not. This result explains in part the usefulness of backward detuning to obtain single solitons [52] and underlines the crucial role that thermal effects play.

When thermal effects can be neglected, as in the experiments of Moille et al. [50], we previously showed that a broad bandwidth frequency comb can be obtained deterministically by appropriately moving through the $\alpha \times F$ [(frequency detuning)×(pump amplitude)] parameter space. First, one raises the pump power. Below the red-dashed curve, a continuous wave is generated that increases in amplitude as the pump amplitude increases. When the red-dashed curve is crossed, the continuous wave becomes unstable, and a cnoidal wave is generated. When $L = 50$, this cnoidal wave has periodicity 8, corresponding to the solid black curve labeled 8 in Fig. 1(a). When it appears, this cnoidal wave corresponds to a narrowband frequency comb so that in the azimuthal domain there is a periodic array of eight peaks that sits atop a pedestal, as shown in Fig. 2(c). Next, one increases the detuning while simultaneously raising the pump power so that the system remains within the stable region for the cnoidal wave that was created. As the detuning and pump power are increased, the pedestal decreases and the peaks sharpen, so that the cnoidal wave transforms into a periodic train of solitons that is a soliton crystal, as shown in Fig. 2(e) [26,40–49].
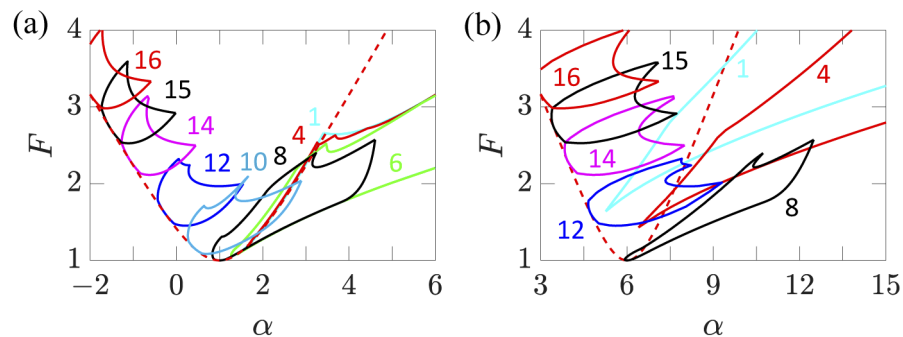

Fig. 1. Stable regions of cnoidal waves (a) without ($C = 0$) and (b) with thermal effects ($C = 5$) at $L = 50$. For clarity, only a selection of the stable regions is plotted. Numbers label the periodicity N of the cnoidal waves. The dashed red curves show a limit below which continuous waves are stable. The scale for α is both shifted to larger values and scaled by a factor 1.5 in (b) relative to (a).

When thermal effects are taken into account, this deterministic path must be somewhat modified. In Fig. 2(a), there is a triangular-shaped region surrounded by blue dashes on two sides and the red-dashed curve on the right. Inside this region, two stable continuous wave solutions exist with different amplitudes. If this region is reached by passing through the lower blue-dashed curve, only the lower amplitude solution is observed. In that case, if one enters the region where the cnoidal waves are stable, which is surrounded by the solid black curve in Fig. 2(a),
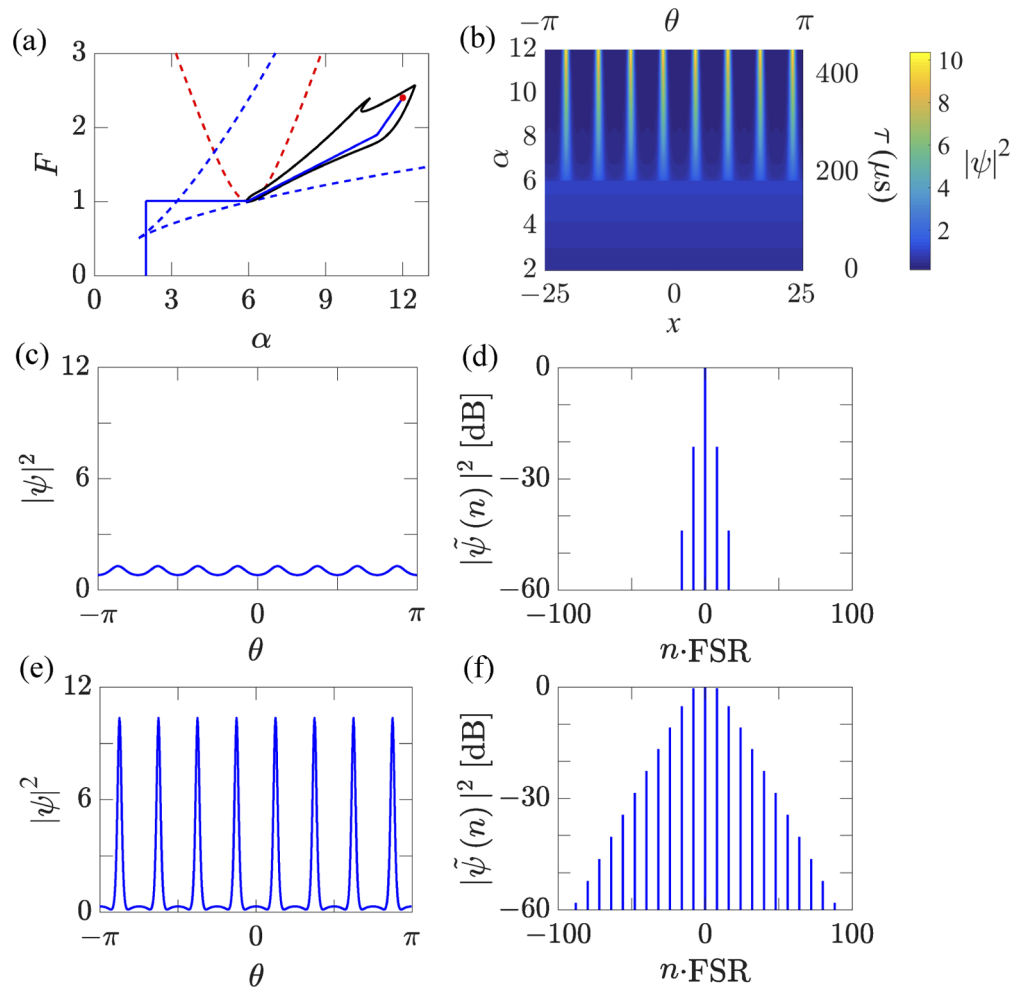
Fig. 2. (a) Stable region of periodicity-8 cnoidal waves including thermal effects with $L = 50$ and $C = 5$ (black curve). The red-dashed curve shows a limit below which continuous waves are stable. The blue-dashed curves show the limits inside of which three continuous wave solutions exist that can be stable or unstable. Inside the triangular-shaped region surrounded by the blue dashes on two sides and the red-dashed curve on the right is a region where two stable continuous wave solutions exist with different amplitudes. (b) Evolution of the waveform when deterministically accessing the periodicity-8 cnoidal wave along the solid blue path, shown in (a). (c) Waveform of the periodicity-8 cnoidal wave and (d) its corresponding spectrum at $\alpha = 6$ and $F = 1.01$. (e) Waveform of the periodicity-8 cnoidal wave and (f) its corresponding spectrum at $\alpha = 12$ and $F = 2.4$ [red dot in (a)].

the continuous wave remains stable, and a cnoidal wave is not observed [55]. Instead, one must enter the triangular region through the upper blue-dashed curve. In that case, a higher-amplitude continuous wave is observed, which goes unstable when the region where cnoidal waves exist is entered, so that the periodicity-8 cnoidal wave is obtained, corresponding to a narrowband frequency comb [55]. Continuing to increase α and F along the solid blue path shown in Fig. 2(a), the peaks become more narrow and the pedestal between the peaks decreases, so that the waveform gradually transforms into a soliton crystal, corresponding to a broadband frequency comb. The solid blue path shown in Fig. 2(a) has a bend. The purpose of this bend is for the path

to remain within the stable region for the periodicity-8 cnoidal wave. It is possible to reach this point without a bend by moving along the solid blue curve in Fig. 3(a). In this case, a cnoidal wave with periodicity 10 first appears. As the system evolves along the solid blue curve, the periodicity-10 cnoidal wave first goes unstable, yielding a periodicity-9 cnoidal wave, which goes unstable in turn, yielding a periodicity-8 cnoidal wave. We show the evolution of the waveform in Fig. 3(b). At the time indicated by the white dashed line, we no longer change α and F, but continue the evolution to ensure that we have reached a stable solution. Other paths through the parameter space that end at the same (α, F) also yield the same broadband cnoidal wave. The key requirements are to enter the triangular region in Figs. 2(a) and 3(a) through the upper dashed curve and to move adiabatically through the parameter space so that the microresonator is always close to thermal equilibrium.
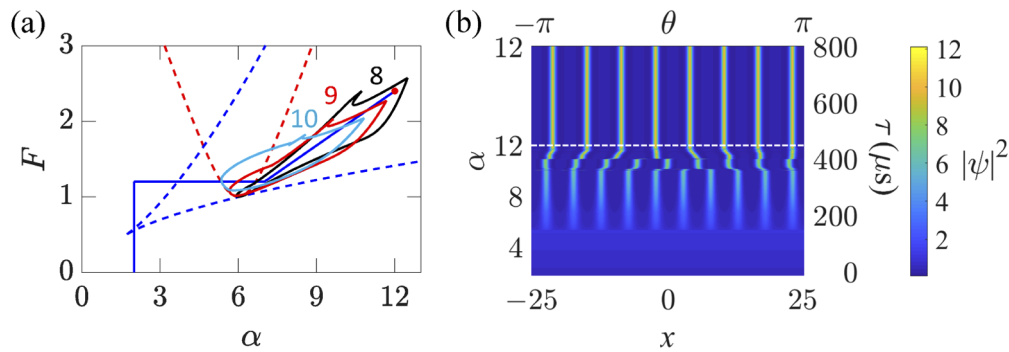

Fig. 3. (a) Stable regions of periodicity-8 (black), -9 (red) and -10 (cyan) cnoidal waves including thermal effects with $L = 50$ and $C = 5$. (b) The evolution to access periodicity-8 cnoidal waves along the solid blue path in (a). Once the path reaches $\alpha = 12$, we continue the evolution without changing α.

The simulations that we carried out to access the broadband cnoidal wave that we show in Figs. 2(b) and 3(b) were carried out adiabatically. To verify that the rate at which we changed the system parameters is slow enough to be adiabatic, we carried out simulations in which we move through the parameter space at half the rate in physical time that we used in Figs. 2(b) and 3(b). Hence, the simulation was twice as long in physical time. We show the results in Fig. 4. While details of the transient evolution change, particularly along the path that we show in Fig. 3(a), the end result does not change except for an azimuthal shift.
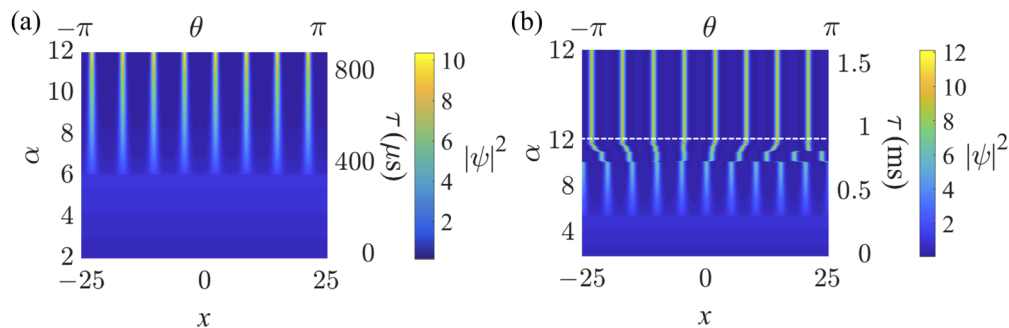

Fig. 4. Simulations at half the rate and twice the duration as in (a) Fig. 2(b) and (b) Fig. 3(b). As was the case in Fig. 3(b), we continue the evolution in Fig. 4(b) without changing α beyond the time indicated by the white-dashed line.

We also compare the stability maps for different values of the thermal parameter C and longitudinal mode circumference L. Figure 5 shows the stable regions for cnoidal waves for (a) $C = 3.42$ and $L = 20$, (b) $C = 5$ and $L = 40$, and (c) $C = 5$ and $L = 70$, which correspond to the experimental parameters in [50], [54], and [13], respectively. Comparing Figs. 5(b) and 5(c), the expected linear scaling of the periodicity of the stable regions is clearly visible. This approximate scaling is somewhat less visible when comparing Fig. 5(a) with the others, both because the scaling becomes less exact when L decreases and because we used a different value of C in Fig. 5(a) in order to better match the experiments in [50].
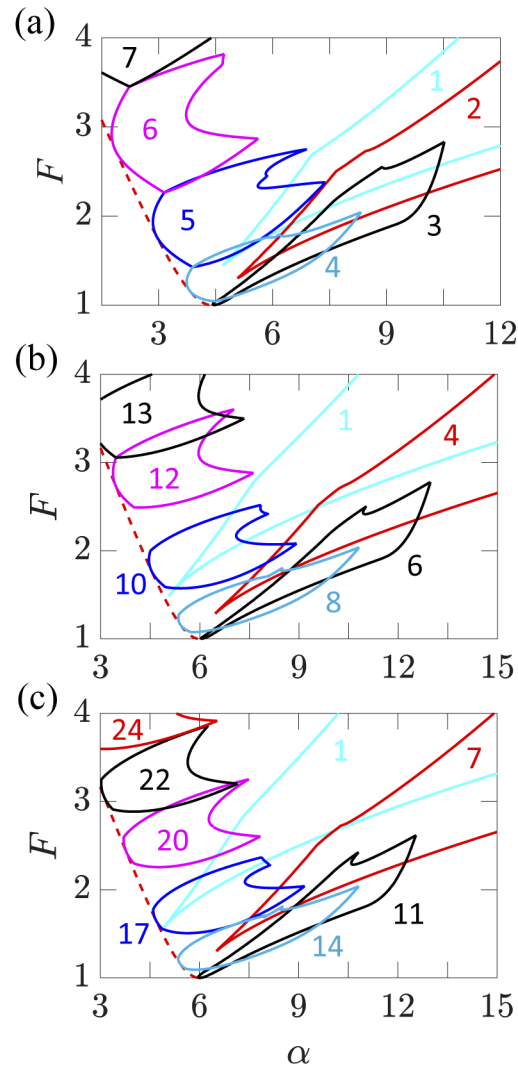

Fig. 5. Stable regions for cnoidal waves with different values of the thermal parameter C and longitudinal mode circumference L: (a) $C = 3.42$ and $L = 20$, (b) $C = 5$ and $L = 40$, (c) $C = 5$ and $L = 70$. In (b) and (c), we only show a selection of the stable regions for clarity. Numbers label the periodicity N.

Figure 6 shows the stable regions for three different values of C for periodicity-8 cnoidal waves when $L = 50$. As C increases, stable regions move to larger α. They are also skewed to larger α

as F becomes larger, which is expected since a larger F corresponds to a larger intracavity power P and hence a larger change in α.
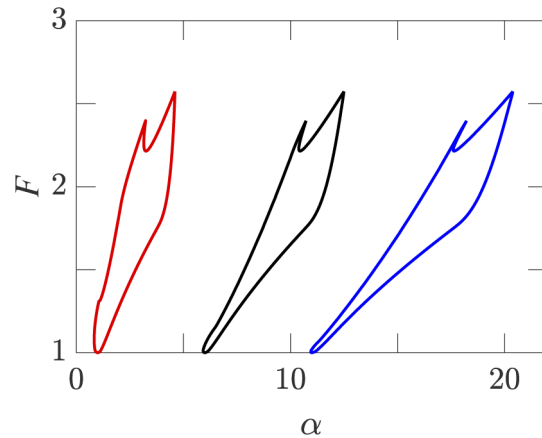

Fig. 6. Stable regions for periodicity-8 cnoidal waves with different values of the thermal parameter C and with $L = 50$. The numbers label the thermal parameter C.

4. Conclusion

We have described a method to deterministically access broad bandwidth frequency combs in microresonators by moving adiabatically through the $\alpha \times F$ [(frequency detuning)×(pump amplitude)] parameter space. This method produces frequency combs that consist of cnoidal waves with periodicity greater than 1. In the broad bandwidth limit, the frequency comb corresponds to a periodic train of solitons that is a soliton crystal.

Thermal effects play a critical role in microresonators and must be taken into account. When thermal effects can be ignored, it is possible to deterministically access broadband combs by first raising the pump power to enter the stable region for cnoidal waves and then simultaneously increasing the detuning and pump power in an appropriate ratio. When thermal effects are taken into account, it is necessary to raise the pump power and then increase the detuning along a path in the parameter space that produces a high-amplitude continuous wave. From that point in the parameter space, it is possible to access broad bandwidth cnoidal waves that are soliton crystals by simultaneously increasing the detuning and pump power along an appropriate path in the parameter space.

While our examples have mostly focused on $L = 50$, there is a scaling relation that makes it possible to extend our results to a large range of L values, and our results indicate that it is possible to deterministically obtain broad bandwidth frequency combs in any microresonator by moving adiabatically through an appropriate path in the $\alpha \times F$ parameter space.

When thermal effects can be neglected, it was previously shown that the stable regions for cnoidal waves in the $\alpha \times F$ parameter space almost completely overlap for small periodicities. In this limit, which corresponds to broadband frequency combs, the cnoidal waves are single solitons or soliton crystals. When thermal effects are important, the stable regions for soliton crystals with different periodicities separate. This result suggests that it may be possible to deterministically obtain single solitons by backwards-detuning from a soliton crystal. This suggestion is compatible with the experimental results of Guo et al. [52] that show that single solitons can be obtained by backwards-detuning from a random array of solitons and by Karpov et al. [46] that show that it is possible to deterministically move in the $\alpha \times F$ parameter space from one soliton crystal to another. We have found that it is indeed possible to deterministically

obtain single solitons in some cases, but we reserve a detailed discussion of this issue for the future.

The work in this paper extends prior work [26] to include thermal effects in a map of the stable regions for cnoidal waves in microresonators. However there are important effects that remain to be included. Chief among them are avoided crossings and higher-order chromatic dispersion, particularly in the broadband limit. Frequency dependence of the coupling, nonlinear, and thermal coefficients in the broadband limit are also likely to be important. These are important topics for future work.

Funding

Acknowledgment

Disclosures

The authors declare no conflicts of interest.

References

1. S. Cundiff, J. Ye, and J. Hall, "Rulers of light," Sci. Am. **298**(4), 74–81 (2008).
2. S. A. Diddams, "The evolving optical frequency comb," J. Opt. Soc. Am. B **27**(11), B51–B62 (2010).
3. S. A. Diddams, K. Vahala, and T. Udem, "Optical frequency combs: coherently uniting the electromagnetic spectrum," Science **369**(6501), eaay3676 (2020).
4. P. Del'Haye, A. Schliesser, O. Arcizet, T. Wilken, R. Holzwarth, and T. J. Kippenberg, "Optical frequency comb generation from a monolithic microresonator," Nature **450**(7173), 1214–1217 (2007).
5. T. J. Kippenberg, R. Holzwarth, and S. A. Diddams, "Microresonator-Based Optical Frequency Combs," Science **332**(6029), 555–559 (2011).
6. A. L. Gaeta, M. Lipson, and T. J. Kippenberg, "Photonic-chip-based frequency combs," Nat. Photonics **13**(3), 158–169 (2019).
7. T. Kippenberg, S. Spillane, and K. Vahala, "Kerr-Nonlinearity Optical Parametric Oscillation in an Ultrahigh-Q Toroid Microcavity," Phys. Rev. Lett. **93**(8), 083904 (2004).
8. A. Savchenkov, A. Matsko, D. Strekalov, M. Mohageg, V. Ilchenko, and L. Maleki, "Low Threshold Optical Oscillations in a Whispering Gallery Mode CaF$_2$ Resonator," Phys. Rev. Lett. **93**(24), 243905 (2004).
9. Y. K. Chembo and N. Yu, "Modal expansion approach to optical-frequency-comb generation with monolithic whispering-gallery-mode resonators," Phys. Rev. A **82**(3), 033801 (2010).
10. Y. K. Chembo, D. V. Strekalov, and N. Yu, "Spectrum and Dynamics of Optical Frequency Combs Generated with Monolithic Whispering Gallery Mode Resonators," Phys. Rev. Lett. **104**(10), 103902 (2010).
11. T. Herr, K. Hartinger, J. Riemensberger, C. Y. Wang, E. Gavartin, R. Holzwarth, M. L. Gorodetsky, and T. J. Kippenberg, "Temporal solitons in optical microresonators," Nat. Photonics **8**(2), 145–152 (2014).
12. M. R. E. Lamont, Y. Okawachi, and A. L. Gaeta, "Route to stabilized ultrabroadband microresonator-based frequency combs," Opt. Lett. **38**(18), 3478–3481 (2013).
13. X. Yi, Q.-F. Yang, K. Y. Yang, M.-G. Suh, and K. Vahala, "Soliton frequency comb at microwave rates in a high-Q silica microresonator," Optica **2**(12), 1078–1085 (2015).
14. P.-H. Wang, J. A. Jaramillo-Villegas, Y. Xuan, X. Xue, C. Bao, D. E. Leaird, M. Qi, and A. M. Weiner, "Intracavity Characterization of Micro-Comb Generation in the Single-Soliton Regime," Opt. Express **24**(10), 10890–10897 (2016).
15. A. Coillet, I. Balakireva, R. Henriet, K. Saleh, L. Larger, J. M. Dudley, C. R. Menyuk, and Y. K. Chembo, "Azimuthal Turing Patterns, Bright and Dark Cavity Solitons in Kerr Combs Generated With Whispering-Gallery-Mode Resonators," IEEE Photonics J. **5**(4), 6100409 (2013).
16. J. Pfeifle, A. Coillet, R. Henriet, K. Saleh, P. Schindler, C. Weimann, W. Freude, I. V. Balakireva, L. Larger, C. Koos, and Y. Chembo, "Optimally coherent Kerr combs generated with crystalline whispering gallery mode resonators for ultrahigh capacity fiber communications," Phys. Rev. Lett. **114**(9), 093902 (2015).
17. V. Brasch, M. Geiselmann, T. Herr, G. Lihachev, M. H. P. Pfeiffer, M. L. Gorodetsky, and T. J. Kippenberg, "Photonic chip-based optical frequency comb using soliton Cherenkov radiation," Science **351**(6271), 357–360 (2016).

18. X. Yi, Q.-F. Yang, K. Y. Yang, and K. Vahala, "Active capture and stabilization of temporal solitons in microresonators," Opt. Lett. **41**(9), 2037–2040 (2016).
19. Q. Li, T. C. Briles, D. A. Westly, T. E. Drake, J. R. Stone, B. R. Ilic, S. A. Diddams, S. B. Papp, and K. Srinivasan, "Stably accessing octave-spanning microresonator frequency combs in the soliton regime," Optica **4**(2), 193–203 (2017).
20. D. T. Spencer, T. Drake, T. C. Briles, J. Stone, L. C. Sinclair, C. Frederick, Q. Li, D. Westly, B. R. Ilic, A. Bluestone, N. Volet, T. Komljenovic, L. Chang, S. H. Lee, D. Y. Oh, M.-G. Suh, K. Y. Yang, M. H. P. Pfeiffer, T. J. Kippenberg, E. Norberg, L. Theogarajan, K. Vahala, N. R. Newbury, K. Srinivasan, J. E. Bowers, S. A. Diddams, and S. Papp, "An optical-frequency synthesizer using integrated photonics," Nature **557**(7703), 81–85 (2018).
21. W. Weng, E. Lucas, G. Lihachev, V. E. Lobanov, H. Guo, M. L. Gorodetsky, and T. J. Kippenberg, "Spectral purification of microwave signals with disciplined dissipative Kerr solitons," Phys. Rev. Lett. **122**(1), 013902 (2019).
22. E. Lucas, P. Brochard, R. Bouchand, S. Schilt, T. Sudmeyer, and T. J. Kippenberg, "Ultralow-noise photonic microwave synthesis using a soliton microcomb-based transfer oscillator," Nat. Commun. **11**(1), 374 (2020).
23. M.-G. Suh, Q.-F. Yang, K. Y. Yang, X. Yi, and K. J. Vahala, "Microresonator soliton dual-comb spectroscopy," Science **354**(6312), 600–603 (2016).
24. M.-G. Suh and K. J. Vahala, "Soliton microcomb range measurement," Science **359**(6378), 884–887 (2018).
25. P. Trocha, M. Karpov, D. Ganin, M. H. P. Pfeiffer, A. Kordts, S. Wolf, J. Krockenberger, P. Marin-Palomo, C. Weimann, S. Randel, W. Freude, T. J. Kippenberg, and C. Koos, "Ultrafast optical ranging using microresonator soliton frequency combs," Science **359**(6378), 887–891 (2018).
26. Z. Qi, S. Wang, J. Jaramillo-Villegas, M. Qi, A. M. Weiner, G. D'Aguanno, T. F. Carruthers, and C. R. Menyuk, "Dissipative cnoidal waves (Turing rolls) and the soliton limit in microring resonators," Optica **6**(9), 1220–1232 (2019).
27. C. Joshi, J. K. Jang, K. Luke, X. Ji, S. A. Miller, A. Klenner, Y. Okawachi, M. Lipson, and A. L. Gaeta, "Thermally controlled comb generation and soliton modelocking in microresonators," Opt. Lett. **41**(11), 2565–2568 (2016).
28. D. V. Strekalov and N. Yu, "Generation of optical combs in a whispering gallery mode resonator from a bichromatic pump," Phys. Rev. A **79**(4), 041805 (2009).
29. T. Hansson and S. Wabnitz, "Bichromatically pumped microresonator frequency combs," Phys. Rev. A **90**(1), 013811 (2014).
30. G. D'Aguanno and C. R. Menyuk, "Nonlinear mode coupling in whispering-gallery-mode resonators," Phys. Rev. A **93**(4), 043820 (2016).
31. G. D'Aguanno and C. R. Menyuk, "Coupled Lugiato-Lefever equation for nonlinear frequency comb generation at an avoided crossing of a microresonator," Eur. Phys. J. D **71**(3), 74 (2017).
32. H. Taheri, A. A. Eftekhar, K. Wiesenfeld, and A. Adibi, "Soliton formation in whispering-gallery-mode resonators via input phase modulation," IEEE Photonics J. **7**(2), 1–9 (2015).
33. C. Bao, P. Liao, A. Kordts, L. Zhang, M. Karpov, M. H. P. Pfeiffer, Y. Cao, Y. Yan, A. Almaiman, G. Xie, A. Mohajerin-Ariaei, L. Li, M. Ziyadi, S. R. Wilkinson, M. Tur, T. J. Kippenberg, and A. E. Willner, "Dual-pump generation of high-coherence primary Kerr combs with multiple sub-lines," Opt. Lett. **42**(3), 595–598 (2017).
34. D. C. Cole, J. R. Stone, M. Erkintalo, K. Y. Yang, X. Yi, K. J. Vahala, and S. B. Papp, "Kerr-microresonator solitons from a chirped background," Optica **5**(10), 1304–1310 (2018).
35. E. Obrzud, S Lecomte, and T. Herr, "Temporal solitons in microresonators driven by optical pulses," Nat. Photonics **11**(9), 600–607 (2017).
36. S. A. Miller, Y. Okawachi, S. Ramelow, K. Luke, A. Dutt, A. Farsi, A. L. Gaeta, and M. Lipson, "Tunable frequency combs based on dual microring resonators," Opt. Express **23**(16), 21527–21540 (2015).
37. B. Y. Kim, Y. Okawachi, J. K. Jang, M. Yu, X. Ji, Y. Zhao, C. Joshi, M. Lipson, and A. L. Gaeta, "Turn-key, high-efficiency Kerr comb source," Opt. Lett. **44**(18), 4475–4478 (2019).
38. X. Xue, Y. Xuan, P.-H. Wang, Y. Liu, D. E. Leaird, M. Qi, and A. M. Weiner, "Normal-dispersion microcombs enabled by controllable mode interactions," Laser Photonics Rev. **9**(4), L23–L28 (2015).
39. C. Bao, Y. Xuan, D. E. Leaird, S. Wabnitz, M. Qi, and A. M. Weiner, "Spatial mode-interaction induced single soliton generation in microresonators," Optica **4**(9), 1011–1015 (2017).
40. D. C. Cole, E. S. Lamb, P. Del'Haye, S. A. Diddams, and S. B. Papp, "Soliton crystals in Kerr resonators," Nat. Photonics **11**(10), 671–676 (2017).
41. Z. Qi, G. D'Aguanno, and C. R. Menyuk, "Nonlinear frequency combs generated by cnoidal waves in microring resonators," J. Opt. Soc. Am. B **34**(4), 785–794 (2017).
42. W. Wang, Z. Lu, W. Zhang, S. T. Chu, B. E. Little, L. Wang, X. Xie, M. Liu, Q. Yang, L. Wang, J. Zhao, G. Wang, Q. Sun, Y. Liu, Y. Wang, and W. Zhao, "Robust soliton crystals in a thermally controlled microresonator," Opt. Lett. **43**(9), 2002–2005 (2018).
43. Z. Lu, W. Wang, W. Zhang, M. Liu, L. Wang, S. T. Chu, B. E. Little, J. Zhao, X. Wang, and W. Zhao, "Raman self-frequency-shift of soliton crystal in a high index doped silica micro-ring resonator," Opt. Mater. Express **8**(9), 2662–2669 (2018).
44. Y. He, Q.-F. Yang, J. Ling, R. Luo, H. Liang, M. Li, B. Shen, H. Wang, K. Vahala, and Q. Lin, "Self-starting bi-chromatic LiNbO$_3$ soliton microcomb," Optica **6**(9), 1138–1144 (2019).
45. A. Coillet, Z. Qi, I. V. Balakireva, G. Lin, C. R. Menyuk, and Y. Chembo, "On the transition to secondary Kerr combs in whispering-gallery mode resonators," Opt. Lett. **44**(12), 3078–3081 (2019).

46. M. Karpov, M. H. P. Pfeiffer, H. Guo, W. Weng, J. Liu, and T. J. Kippenberg, "Dynamics of soliton crystals in optical microresonators," Nat. Phys. **15**(10), 1071–1077 (2019).

47. Y. He, J. Ling, M. Li, and Q. Lin, "Perfect soliton crystals on demand," Laser Photonics Rev. **14**(8), 1900339 (2020).

48. Z. Wu, Y. Gao, J. Dai, T. Zhang, and K. Xu, "Switching dynamics of reconfigurable perfect soliton crystals in dual-coupled microresonators," arXiv:2007.15557 (2020).

49. P. Parra-Rivas, D. Gomila, L. Gelens, and E. Knobloch, "Bifurcation structure of localized states in the Lugiato-Lefever equation with anomalous dispersion," Phys. Rev. E **97**(4), 042204 (2018).

50. G. Moille X. Lu, A. Rao, Q. Li, D. A. Westly, L. Ranzani, S. B. Papp, M. Soltani, and K. Srinivasan, "Kerr-Microresonator Soliton Frequency Combs at Cryogenic Temperatures," Phys. Rev. Appl. **12**(3), 034057 (2019).

51. Z. Qi, J. Jaramillo-Villegas, G. D'Aguanno, T. F. Carruthers, O. Gat, A. M. Weiner, and C. R. Menyuk, "A Deterministic Method for Obtaining Large-Bandwidth Frequency Combs in Microresonators with Thermal Effects," in *Conference on Lasers and Electro-Optics* (Optical Society of America, 2020), paper SW4J.5.

52. H. Guo, M. Karpov, E. Lucas, A. Kordts, M. H. P. Pfeiffer, V. Brasch, G. Lihachev, V. E. Lobanov, M. L. Gorodetsky, and T. J. Kippenberg, "Universal dynamics and deterministic switching of dissipative Kerr solitons in optical microresonators," Nat. Phys. **13**(1), 94–102 (2017).

53. S. Diallo, G. Lin, and Y. K. Chembo, "Giant thermo-optical relaxation oscillations in millimeter-size whispering gallery mode disk resonators," Opt. Lett. **40**(16), 3834–3837 (2015).

54. C. Bao, Y. Xuan, J. A. Jaramillo-Villegas, D. E. Leaird, M. Qi, and A. M. Weiner, "Direct soliton generation in microresonators," Opt. Lett. **42**(13), 2519–2522 (2017).

55. A. Leshem, Z. Qi, T. F. Carruthers, C. R. Menyuk, and O. Gat, "Thermal instabilities, frequency comb formation, and temporal oscillations in Kerr microresonators," submitted to Phys. Rev. A (2020).